OATAO
Open Archive Toulouse Archive Ouverte

Open Archive Toulouse Archive Ouverte (OATAO)

OATAO is an open access repository that collects the work of Toulouse researchers and makes it freely available over the web where possible

Hydroxyapatite functionalization to trigger adsorption and release of risedronate

Lucia Forte[a], Stéphanie Sarda[b], Christèle Combes[c], Fabien Brouillet[d], Massimo Gazzano[e], Olivier Marsan[c], Elisa Boanini[a,*], Adriana Bigi[a]

[a] *Department of Chemistry "G. Ciamician", University of Bologna, via Selmi 2, 40126 Bologna, Italy*
[b] *CIRIMAT, INPT-CNRS-UPS, Université de Toulouse, Université Paul Sabatier, 4 allée Emile Monso, 31030 Toulouse cedex 4, France*
[c] *CIRIMAT, INPT-CNRS-UPS, Université de Toulouse, ENSIACET, 4 allée Emile Monso, 31030 Toulouse cedex 4, France*
[d] *CIRIMAT, INPT-CNRS-UPS, Université de Toulouse, Faculté des Sciences Pharmaceutiques, 35 Chemin des Maraichers, 31062 Toulouse cedex 9, France*
[e] *ISOF-CNR, Via Gobetti 101, 40129, Bologna, Italy*

ARTICLE INFO

ABSTRACT

Bisphosphonates are widely employed drugs for the treatment of pathologies characterized by excessive bone resorption, and display a great affinity for apatitic supports. In this work we investigate how hydroxyapatite functionalization can influence the processes of adsorption and release of a bisphosphonate, namely risedronate. To this aim, pure hydroxyapatite (HA), hydroxyapatite with a partial substitution of Zn to Ca (ZnHA) and poly-ethylenimine-functionalized hydroxyapatite (HAPEI) were submitted to interaction with risedronate solution. The results indicate that the mechanisms of adsorption and release are greatly influenced by the type of the apatitic support. All the apatitic supports display Langmuir isotherms for risedronate adsorption. However in the case of HAPEI the plateau is not reached even at high equilibrium concentrations in solution. The data suggest that risedronate adsorption on HAPEI mineral-organic support occurs not only through chemisorption on apatitic phase, as on HA and ZnHA, but also through physisorption involved by PEI coating, which modulates also bisphosphonate release. These properties of tailor-made hydroxyapatite supports could be exploited to develop delivery systems for antiresorptive agents directly on osteoporotic sites.

1. Introduction

Bisphosphonates (BPs) are widely and successfully employed for the treatment of diseases associated to bone turn-over disorders related to pathologies, such as osteoporosis, Paget's disease and bone metastases [1,2]. In fact, these drugs not only display a great affinity for the mineral phase of bone, preventing its dissolution, but also inhibit osteoclast activity [3]. However, their systemic prolonged use has been shown to provoke several negative side effects, including jaw osteonecrosis, gastrointestinal disorders, atypical subtrochanteric fractures [2,4,5]. Moreover a low bioavailability is commonly observed for oral administration. Local release at specific bone sites exhibiting a risk of fractures has been suggested as a promising alternative strategy to deliver BPs without incurring in undesirable side effects [2]. Several supports have been proposed in the literature and apatitic calcium phosphates appear as good candidates as they are similar to bone mineral and largely used for bone substitute applications [6–13]. BPs-functionalized CaPs can be prepared through adsorption from solution, as well as by direct synthesis in aqueous solution [9,12,13]. A study carried out by Nancollas et al. using a constant composition method allowed to determine the binding affinity of several BPs to hydroxyapatite (HA) [14]. Moreover, previous studies on the mechanism of adsorption and desorption processes evidence the influence of the structure and composition of the apatitic surface on the parameters of adsorption of BPs and their kinetics of release [13,15,16].

In this study we investigated the role of composition and surface charge of hydroxyapatite supports on the adsorption and release mechanisms of risedronate. To this aim, we utilized HA, HA with a partial substitution of zinc to calcium (ZnHA), and HA functionalized with polyethyleneimine (HAPEI). PEI and Zn can indeed fulfill different useful roles. PEI is a polycationic polymer containing a high density of ionizable amino groups, widely employed to coat HA for chromatographic applications and complex transfection systems [17–19]. Herein we synthesized hydroxyapatite in the presence of PEI in solution in order to get functionalized HA crystals

with an increased number of positive charges on their surface with respect to pure HA. Enhancement of positive charge on the surface of the HA nanocrystals, thanks to the presence of the polycationic polymer, should promote the adsorption of negatively charged BPs from solution and control their release.

On the other hand, cationic substitution in HA can influence crystal growth and increase the specific surface area which in turn controls the adsorption ability [20]. Zinc can partially substitute for calcium in the structure of HA and has been demonstrated to inhibit osteoclast formation and bone resorption [20,21]. Its presence into HA structure might influence BPs interaction with the calcium phosphate surface. Moreover its co-presence with BPs in HA crystals should enhance the antiresorptive properties of the material.

In the present paper, we investigated the interaction between risedronate and different apatitic crystals (HA, HAPEI and ZnHA), through the study of the adsorption reaction of this BP on these different apatitic supports and physicochemical characterization of the solid products and of the supernatant solutions. Then, the release of risedronate from the three types of apatitic supports will be studied and discussed.

2. Materials and methods

2.1. Synthesis of the apatitic samples

The synthesis of HA was carried out in N_2 atmosphere using CO_2 free water [22]. 50 mL of a 1.08 M $Ca(NO_3)_2·4H_2O$ solution (pH adjusted to 10 with NH_4OH) was heated at 90 °C and 50 mL of 0.65 M $(NH_4)_2HPO_4$ solution was added drop-wise under stirring. The precipitate was maintained in contact with the reaction solution for 5 h at 90 °C under stirring, then centrifuged at 10,000 rpm for 10 min and repeatedly washed with CO_2-free distilled water. The product was dried at 37 °C overnight.

Hydroxyapatite at different poly(ethylenimine) contents (HAPEI) was obtained following the same experimental procedure as for HA except that PEI was added to the $Ca(NO_3)_2·4H_2O$ solution, before adjusting the pH to 10 with NH_4OH. Poly(ethylenimine) solution (Aldrich, MW $\sim$ 2000 g mol^{-1}) was used. Concentrations of PEI tested were 1, 2 and 4 M (calculated with respect to the final volume of the precipitating medium) leading to HAPEI 1, HAPEI 2 and HAPEI 4 samples, respectively.

Zn-substituted hydroxyapatite (ZnHA) was synthesized following the same experimental procedure as for HA, but the cationic solution was prepared by dissolving the appropriate amounts of $Ca(NO_3)_2·4H_2O$ and $Zn(NO_3)_2·6H_2O$ in CO_2-free deionized water before adjusting the pH to 10 with NH_4OH. The total cationic concentration was 1.08 M, and the $Zn/(Ca + Zn)$ molar ratio was 0.1.

2.2. Risedronate adsorption and release

Adsorption experiments were carried out on HA, ZnHA and HAPEI. The HAPEI samples used for risedronate adsorption study was HAPEI 4, from now onwards indicated as HAPEI for simplicity. 50 mg of apatitic sample were dispersed at physiological temperature (37 ± 1 °C) in 5 mL of risedronate (Aldrich) solutions (concentration ranging from 0 to 3 mM) in a polyethylene tube. The latter were prepared by dissolving the appropriate amount of risedronate in an aqueous 1 mM KCl solution (standard solution); the pH of the obtained solutions was adjusted to 7.4 using HCl or KOH solutions. After sonication for 1 min, the suspensions were incubated for 1 h without stirring and then centrifuged for 10 min at 5000 rpm leading to the various BP-functionalized apatites: HABP, HAPEIBP and ZnHABP samples. This equilibration time (1 h) was previously determined from kinetic experiments

using a risedronate solution of 0.86 mM; this time allowed to reach the equilibrium of adsorption while minimizing the dissolution of apatitic supports. Blanks containing only apatite incubated in KCl solutions were used as controls. After centrifugation, the solids obtained were washed with deionized water and dried at 37 °C overnight. The supernatants were immediately filtrated on 0.2 μm Millipore filters and then stored at 4 °C before titration.

The risedronate concentration in the filtrates was determined using UV spectrophotometric absorption at 262 nm (Hewlett Packard 8452 A diode array spectrophotometer). This wavelength corresponds to the maximum absorbance of the pyridine group of risedronate molecule.

Risedronate release profiles were obtained with a flowthrough cell system (USP Apparatus 4 Sotax CE6, Sotax AG, Switzerland) with 12 mm cells for powders and a peristaltic pump. In all experiments, laminar flow was used with one glass beads layer covered with each BP-functionalized apatitic sample, mixed with 2 g of glass beads. Different weights were utilized for the analysis of the different materials so that all the samples contained the same amount of adsorbed BP (about 1.8 μmol/m^2). The release tests were carried out at 37.0 ± 0.5 °C under sink conditions according to European Pharmacopeia guidelines. The dissolution medium used was deionized water pumped through the column at a flow rate of 9 mL/min. A closed system was used, recycling 50 mL of dissolution medium. Fractions of 5 mL were collected periodically and risedronate content was determined by UV spectrophotometry at 262 nm. The same volume of dissolution medium was replaced back after each sampling in order to maintain the volume constant and sink conditions. Release study was performed in triplicate for each type of BP-functionalized apatite.

2.3. Sample characterization

X-Ray diffraction analysis was carried out by means of a PANalytical X'Pert PRO powder diffractometer equipped with a fast X'Celerator detector. Ni-filtered CuKα radiation was used (40 mA, 40 kV). The 2θ range was investigated from 10° to 120° with a step size of 0.033° and a time/step of 200 s. The determination of the cell and size/strain parameters was obtained by a full profile pattern refinement using the MAUD (Material Analysis Using Diffraction) routine [23] with the Popa anisotropic size-strain model [24]. The instrumental broadening was estimated by scanning the silicon NIST 640 e sample.

Ca, Zn and P contents in the solid products were determined by means of an inductively coupled plasma (ICP) mass spectrometer (ICP-AES, Horiba Jobin Yvon). Powders were previously dissolved in 0.6 M HNO_3 solution.

The infrared spectrum of each synthesized and functionalized apatite powder was recorded over the 400–4000 cm^{-1} range in transmission mode with KBr pellets (2 mg sample/300 mg KBr) using a Thermo Nicolet 5700 Fourier-transform infrared (FTIR) spectrometer.

Raman spectra of the samples were generated on a Horiba, Jobin-Yvon Labram HR800 confocal microspectrometer, equipped with a helium–neon laser (λ = 632.82 nm). The spectral resolution was 2 cm^{-1}, the laser power was 2 mW and integration times varied from 30 to 120 s. All spectra were recorded over a wavelength range of 100–4000 cm^{-1}. Three spectral accumulations were averaged.

For TEM investigations, a drop of sonicated apatitic calcium phosphate suspension in ethanol was transferred onto holey carbon foils supported on conventional copper microgrids. A Philips CM100 transmission electron microscope, operating at 80 kV was used.

Thermogravimetric analysis was carried out using a PerkinElmer TGA-7. Heating was performed in a platinum crucible in air flow (20 cm^3/min) at a rate of 10 °C/min up to 800 °C.
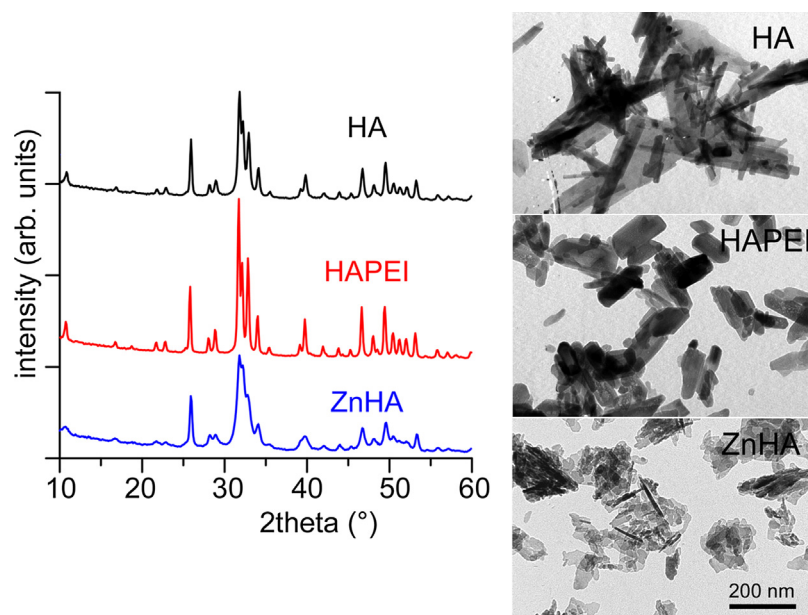
Fig. 1. Powder X-ray diffraction patterns and TEM images of the different synthesized apatitic samples: HA, HAPEI, ZnHA. Magnification in all TEM images is the same for direct comparison.

The sample weights were in the range 5–10 mg. Results from this analysis represent the mean value of determinations for three different samples of each composition.

Zeta potential was measured using a Malvern Instruments Zetasizer Nano. 5 mg of powder sample was suspended in 50 mL of MilliQ water after sonication for 2 min. Each analysis was performed in triplicate.

The specific surface area was measured using a Carlo Erba Sorpty 1750 BET analyzer using constant volume N_2 adsorption with desorption at 80 °C.

3. Results and discussion

3.1. Characterization of the apatitic substrates

Chemical analysis of HA powder gave a Ca/P ratio of 1.67 characteristic of stoichiometric hydroxyapatite (Table S1). The powder XRD patterns of HA, HAPEI (PEI concentration in solution: 4 M) and ZnHA are presented in Fig. 1.

It is evident that all the samples are constituted of apatitic calcium phosphate as unique crystalline phase. However, the broadening of the XRD peaks varies with the type of apatite substrates synthesized. In particular, the reflections in the pattern of HAPEI are more sharp than those of pure hydroxyapatite. We can observe that the products obtained through the synthesis of HA in the presence of different PEI concentrations in solution, namely 1, 2 and 4 M, display an increase of the sharpness of the diffraction peaks on increasing PEI concentration (Fig. S1), which suggests an increase of crystallinity of the apatites precipitated in these conditions. This trend is confirmed by the Raman spectroscopic analysis of these samples (Fig. S2); indeed, the sharpness of the phosphates

and hydroxyl vibration bands characteristic of HA increases on increasing PEI content. Moreover, the spectra of the samples containing the cationic polymer exhibit the presence of two absorption bands around 2800–2900 cm^{-1} characteristic of —CH symmetric and asymmetric stretching bands (—NH stretching vibration band of PEI at about 3300 cm^{-1} cannot be observed probably due to their low intensity) [25].

The lengths of the coherent domains (τ_{hkl}) and the values of microstrain (ε) were calculated from the microstructure parameters determined from the X-ray diffraction pattern refinement procedure. The results show that the main contribution to the broadening of the reflections is due to coherent length of the perfect crystalline domains, which increases significantly both along the c-axis direction and, even more, along the orthogonal direction on increasing PEI content in the solids (Table S1). At variance, the values of microstrain are of the order of 10^{-4} and do not change appreciably as a function of composition. In agreement with the increase of crystallinity, the lattice parameters exhibit a slight but significant reduction of the a-parameter on increasing PEI content [26]. PEI content, determined through thermogravimetric analysis (Fig. S3) increases as a function of concentration in solution up to about 2.5 wt.%. The hypothesis of an electrostatic interaction between the polymer chain (rich in amino groups) and the surface of the apatitic crystals is supported by the values of zeta potential, which assume positive values and increase on increasing the content of the polycationic polymer (Table S1). The presence of PEI associated with apatite nanocrystals influences their morphology: when compared with HA nanocrystals, the HAPEI ones display a shorter mean length and a greater thickness (Fig. 1).

However, the morphological variation does not provoke significant modification of the specific surface area, which is quite similar

Table 1
Lattice parameters, coherent lengths (τ_{hkl}) of the perfect crystalline domains in the direction normal to 002 and to 310 planes; Specific surface area (SSA); Zeta potential; PEI and Zn content of the different apatitic samples synthesized (HA, HAPEI and ZnHA).

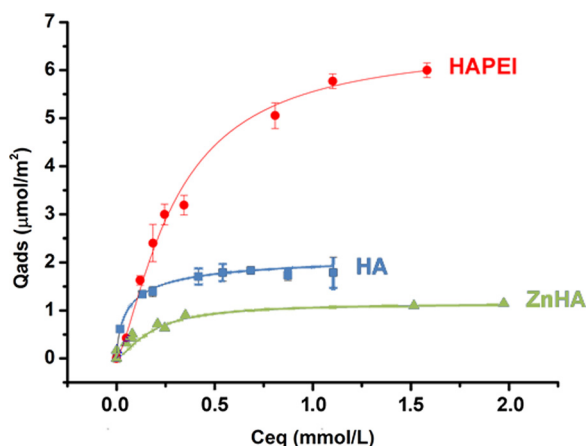|	a (Å)	c (Å)	L 002 (Å)	L 310 (Å)	PEI content (wt.%)	Zn content (at.%)	SSA (m^2/g)	Zeta potential (mV)
HA	9.4378(3)	6.8862(2)	657(4)	311(3)	–	–	23	−15.6
HAPEI	9.4298(2)	6.8872(2)	929(7)	543(5)	2.4	–	26	+26.2
ZnHA	9.4241(9)	6.8696(2)	367(4)	148(3)	–	7.9	86	−15.3

Fig. 2. Adsorption isotherms of risedronate on hydroxyapatite (HA), Zn-substituted hydroxyapatite (ZnHA) and PEI-modified hydroxyapatite (HAPEI) at pH 7.4 and 37 °C. The data fit the Langmuir isotherm.

to that of pure HA (Table 1). On the basis of their increased thickness and coherent length of perfect crystalline domains, it could be suggested that HAPEI nanocrystals can be considered as mesocrystals [27] made up of HA nanoparticles aligned by PEI: PEI could interact preferentially with the hydroxyapatite crystal faces parallel to the c-axis and promote the oriented attachment of nanoparticles, leading to the observed increased thickness (Table 1).

ZnHA nanocrystals exhibit more perturbed shape, ill-defined edges and significantly reduced dimensions in comparison to HA (Fig. 1). Moreover, ZnHA displays a remarkably higher specific surface area when compared to HA and HAPEI, in agreement with its smaller crystal dimensions (Table 1). Zn inhibition of HA crystal growth is in agreement with previous studies [28,29] and it is supported by the observed broadening of the diffraction peaks of ZnHA with respect to those of HA (Fig. 1). Accordingly, the coherent lengths of the perfect crystalline domains of ZnHA evaluated from the line broadening of the (002) and (310) are significantly reduced with respect to those of pure HA (Table 1). Zn incorporation into HA crystals to about 7.9 atom.% provokes a reduction of the lattice parameters, in agreement with its smaller ionic radius with respect to that of calcium [30], with no secondary crystalline phase observed.

3.2. Risedronate adsorption

The evolution of the amount of risedronate adsorbed on the solids Q_{ads} (μmol/m^2) from the dilute solutions as a function of the equilibrium BP concentration C_{eq} (0–2 mM) is plotted in Fig. 2.

The isotherms obtained for HA and ZnHA are Langmuirian in shape ($r^2 = 0.87$ and 0.94, respectively) and reached the plateau at relatively low equilibrium concentrations (below 1 mM), indicating a high affinity of risedronate for these apatitic surfaces. Similar observations have been reported previously for the adsorption of bisphosphonate molecules (risedronate and tiludronate) on apatitic support [13,15,16]. For same weight of apatitic powders, the risedronate content at plateau in presence of ZnHA was twice as much as that adsorbed on HA (about 40 and 100 μmol/g for HA and ZnHA, respectively) mainly due to the higher specific surface area of ZnHA (86 m^2/g) compared with that of HA (23 m^2/g), (Table 1). The uptake of risedronate depended linearly on the amount of released phosphate ions in solution (Fig. S4). Thereby, the uptake of risedronate is proportional to the amount of phosphate ions released in solution indicating that the adsorption of risedronate on HA affects the amount of ionic species in solution and can be described as a chemisorption corresponding to an ion

	$N \pm \Delta N \, (\mu mol/m^2)$	$K \pm \Delta K \, (L\,mmo1^{-1})$
HA	1.88 ± 0.05	21 ± 3
ZnHA	1.20 ± 0.08	7 ± 1
HAPEI	7.9 ± 0.4	2.2 ± 0.3

exchange process between bisphosphonate molecules in solution and phosphates species on HA and ZnHA, as previously published for bisphosphonates adsorption on apatitic surfaces [13–16,31]. The slope of the curve is close to 1 for HA and it increases for ZnHA. Indeed the number of phosphate groups released per adsorbed risedronate molecule varies as a function of the characteristics of the apatitic support, as observed in previous studies on BPs adsorption on apatitic substrates [15,16,31]. It can be noticed that the calcium and zinc concentrations in the supernatants after adsorption were low and not affected by the adsorption of risedronate (Ca concentrations for HA and HAPEI: below 0.5 mM; Zn and Ca concentrations for ZnHA: below 0.5 mM and 2 mM, respectively). These concentrations are related to slight dissolution of the supports during adsorption experiments [16].

The parameters of adsorption can be determined from the Langmuir Eq. (1), (Table 2):

$$Q_{ads} = KNC_{eq} / \left(1 + KC_{eq} \right) \tag{1}$$

where N corresponds to the maximum amount of adsorbed risedronate (μmol/m^2) and K is the affinity constant of risedronate for the solid surface (L/mmol). The values of N obtained for the HA and ZnHA supports are close (Table 2): 1.88 ± 0.05 and $1.20 \pm 0.08 \, \mu$mol/m^2, respectively, and correspond to the values previously obtained for the adsorption of risedronate molecules on apatitic surface [13]. At the same time, a significant decrease of the affinity K is observed for ZnHA (7 ± 1 L/mmol) compared with HA (21 ± 3 L/mmol), (Table 2), possibly related to changes in surface chemical composition.

The isotherm of risedronate adsorption on HAPEI can also be described by the Langmuir model ($r^2 = 0.99$). The amount adsorbed at saturation, N, was higher on HAPEI ($7.9 \pm 0.4 \, \mu$mol/m^2) than on HA and ZnHA but the curve does not reach a plateau even at high equilibrium concentrations in solution (C_{eq}). This can be due to the competition of several processes: a chemisorption process on HA surface and a physisorption process on PEI coating. The decrease of the affinity K for HAPEI (2.2 ± 0.3 L/mmol), (Table 2) can be explained by the presence of PEI on the apatitic surface. The evolution of the amount of risedronate adsorbed as a function of phosphate released in solution is still linear, but the slope appears lower than for HA. The ion exchange process proposed to occur at the surface of the apatite seems to be affected by the presence of PEI. The number of phosphate groups released per BP molecule is lower in the presence of PEI, in agreement with the presence of two different mechanisms of adsorption: risedronate chemisorption, which provokes phosphate release, and risedronate physisorption, which does not imply ion exchange.

3.3. Characterization of the solids after risedronate uptake

The results of XRD analysis of the solid products obtained after bisphosphonate adsorption show that the presence of risedronate does not influence the crystallinity of the apatitic samples and does not provoke precipitation of any other crystalline phase (Fig. S5).
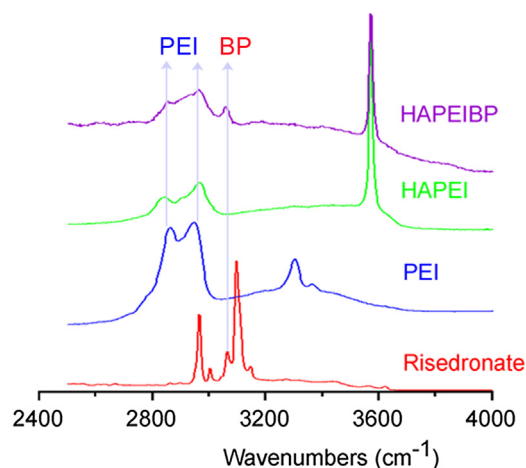
Similarly, TEM images of HABP, ZnHABP and HAPEIBP show that the characteristic morphologies of the different apatitic samples used as substrates for risedronate adsorption are maintained
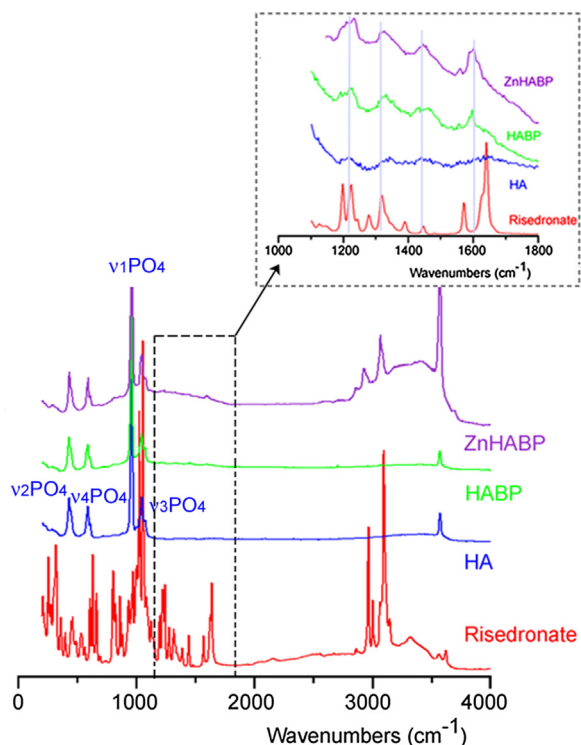
Fig. 3. Raman spectra of risedronate sodium salt, HA, HABP and ZnHABP after adsorption (with Qads equal to the maximum value of the adsorption isotherm).

Fig. 4. Raman spectra of risedronate sodium salt, PEI, HAPEI and HAPEIBP after adsorption (with Qads equal to the maximum value of the adsorption isotherm).

after adsorption, as it can be appreciated by comparing the images reported in Fig. S6 with those in Fig. 1. Adsorption of BP does not significantly modify the values of zeta potential of HA and ZnHA, whereas it provokes a slight, but appreciable, decrease of the zeta potential of HAPEI (from 26.2 to 23.5 mV).

Raman spectra of HA and ZnHA after adsorption (Fig. 3) show the characteristic vibration bands of the apatitic structure [32], especially those of apatitic phosphate groups: ν_2 (438–463 cm^{-1}), ν_4 (580–614 cm^{-1}), ν_1 (960 cm^{-1}), ν_3 (1029–1077 cm^{-1}), and the OH vibration band at 3560 cm^{-1} [33]. All spectra display additional bands which can be attributed to the presence of adsorbed BP: in particular, two bands between 2900 and 3000 cm^{-1}, corresponding to C—H stretching, and two intense bands between 1025 and 1055 cm^{-1} which might be assigned to C—H pyridine ring deformation, are present. Moreover, the spectra show medium intensity bands between 1500 and 1600 cm^{-1}, associated with the substituted pyridine ring, and the characteristic Raman bands of phosphonate groups between 850 and 1230 cm^{-1}. Interestingly, we can see that these bands are shifted compared to those of risedronate sodium salt spectrum, showing a change in the envi-

ronment of these groups after adsorption. These spectroscopic observations suggest a strong interaction between risedronate molecule and calcium ions at the surface of the apatitic samples after adsorption, as no insoluble calcium salts were observed by XRD and TEM (Figs. S5 and S6). These results are in accordance with the Langmuir model proposed for the adsorption isotherm, and the mechanism of interaction based on ion exchange process.

A shift of the characteristic bands of risedronate is also observed in the Raman spectrum of HAPEIBP after adsorption (Fig. 4), which confirmed that the process of adsorption of BP on the mineral part of HAPEI was similar. Moreover the presence of the vibration bands of PEI molecules (especially stretching vibrations of CH, CH$_2$ groups between 2800 and 3000 cm^{-1}) on HAPEIBP confirmed that PEI was still on HA surface after adsorption experiments. Thus, PEI is able to participate to the process of BP adsorption.

3.4. Risedronate release

The results of kinetics of risedronate release from the different apatitic supports are presented in Fig. 5a. The release was fast during the first hour and then slowed down, as observed in previous studies for several apatitic supports [16]. All the samples release a quantity of risedronate that represents a small percentage of the initial adsorbed amount. However, the type of apatitic support is an important parameter for BP release control. In fact, the total amount of risedronate released was higher from HAPEI (about 14% of the initial quantity adsorbed) than from HA and ZnHA (about 5 and 9% respectively) probably due to different processes of release.

In order to describe and correlate the mechanism of BP release from each support, various usual mathematical models were tested
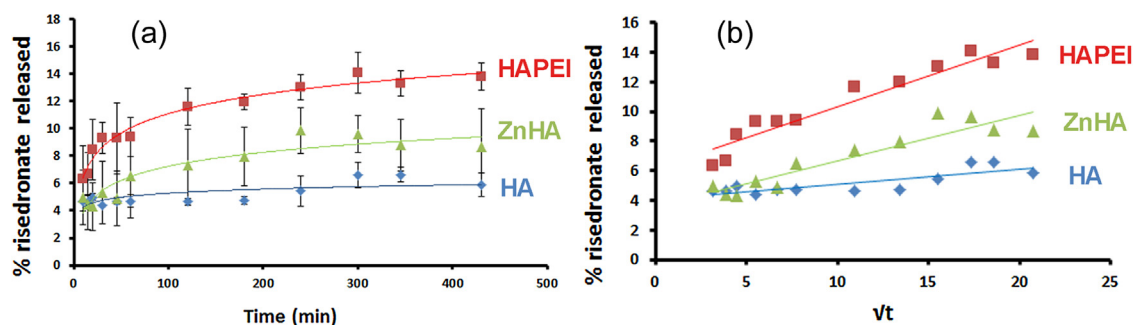
Fig. 5. (a) Risedronate (BP) released (wt.%) from the different apatitic samples as a function of time. The initial amount of BP on each sample was the same, *i.e.* about 1.8 μmol/m^2. (b) Linear regression of Higuchi model (% BP released = K$_H$ × √t, with K$_H$ constant) for the release kinetics of risedronate from HA, ZnHA and HAPEI.

[34]. The results of curve fitting with these models give interesting indications on the release behavior of risedronate from the different tested supports.

First, the release of risedronate from the apatite supports without PEI (HA and ZnHA) cannot be directly described by a simple Higuchi diffusion model ($r^2 = 0.66$ and 0.83 for HA and ZnHA, respectively, Fig. 5b), suggesting another mechanism involving mainly dissolution of the apatitic support [34]. In the case of HA and ZnHA, risedronate molecules were only slowly released from these apatitic supports because they were irreversibly bound by chemisorption. Indeed the exchanged species cannot be removed from apatitic surface by simple dilution of the exchange solution or simple washing of the solids, as previously published for adsorbed molecules on apatites, particularly bisphosphonates [16]. Therefore the release rate was limited by support dissolution keeping in mind the diminishing surface of the apatitic particles during dissolution; the dissolution deceleration may be explained on the basis of the reduction in particle size and surface as observed by several authors for degradation kinetic studies of calcium phosphates [35,36]. Moreover, assuming that the rate of dissolution depends on the surface area of the particle, the higher BP release rate observed from ZnHA compared with HA can be attributed to its higher specific surface area and solubility.

In contrast, the release mechanism from HAPEI seemed governed by simple laws of diffusion ($r^2 = 0.98$ from HAPEI, Fig. 5b) as generally observed from polymeric matrix [34,37]. Liquid penetrates the PEI surface and dissolves the trapped drug, which then diffuses into the release medium. However, if a total delivery of the drugs may be obtained for pure diffusion model applied to pure polymeric supports, it was not observed from HAPEI mineral-organic support (no more than 15% of the initial quantity adsorbed are released after 7 h of test) suggesting the involvement of a secondary mechanism related to the composite nature of the HAPEI. The fast release observed during the first hour can be attributed to the release of the drug molecules associated to the organic phase by physisorption, whereas the following slow release of BP can be ascribed to dissolution of the apatitic phase. This more complex mechanism of release explains the relatively higher quantity of drug delivered from HAPEI compared with those from HA and ZnHA.

4. Conclusions

The results of this study indicate that all the apatitic supports display Langmuir isotherms of adsorption. The mechanism of adsorption can be explained by ionic exchange between bisphosphonate molecules in solution and phosphate on the surface of apatitic supports. The values of the parameters of adsorption, N and K, obtained for the HA and ZnHA supports are close and correspond to the values previously obtained for the adsorption of risedronate molecules on apatitic surfaces.

Interestingly, in the case of HAPEI, the plateau of the Langmuir isotherm of risedronate adsorption was not reached even at high equilibrium concentrations in solution. Risedronate adsorption on HAPEI mineral-organic support occurs not only through chemisorption on apatitic phase, as for HA and ZnHA crystals, but also through physisorption involving PEI coating. Both mechanisms modulate bisphosphonate release. These results show that similarly to the adsorption process, risedronate release is directly related to the nature and the physicochemical characteristics of the apatitic supports. The characteristics and properties of these tailor-made hydroxyapatite supports could be exploited to develop delivery systems for antiresorptive agents directly on osteoporotic sites, allowing reduction of systemic treatments and associated drawbacks.

Appendix A. Supplementary data

Supplementary data associated with this article can be found, in the online version, at https://doi.org/10.1016/j.colsurfb.2017.09.055.

References

[1] R.G.G. Russell, Bisphosphonates: the first 40 years, Bone 49 (2011) 2–19.
[2] M. Fazil, S. Baboota, J.K. Sahni, Ameeduzzafar, J. Ali, Bisphosphonates: therapeutics potential and recent advances in drug delivery, Drug Deliv. 22 (2015) 1–9.
[3] R.G.G. Russell, N.B. Watts, F.H. Ebetino, M.J. Rogers, Mechanisms of action of bisphosphonates: similarities and differences and their potential influence on clinical efficacy, Osteoporos. Int. 19 (2008) 733–759.
[4] G. Favia, G.P. Pilolli, E. Maiorano, Histologic and histomorphometric features of bisphosphonate-related osteonecrosis of the jaws: an analysis of 31 cases with confocal laser scanning microscopy, Bone 45 (2009) 406–413.
[5] R. Rizzoli, K. Åkesson, M. Bouxsein, J.A. Kanis, N. Napoli, S. Papapoulos, J.Y. Reginster, C. Cooper, Subtrochanteric fractures after long-term treatment with bisphosphonates: a European society on clinical and economic aspects of osteoporosis and osteoarthritis, and international osteoporosis foundation working group report, Osteoporos. Int. 22 (2011) 373–390.
[6] S. Josse, C. Faucheux, A. Soueidan, G. Grimandi, D. Massiot, B. Alonso, P. Janvier, S. Laïb, P. Pilet, O. Gauthier, G. Daculsi, J. Guicheux, B. Bujoli, J.M. Bouler, Novel biomaterials for bisphosphonate delivery, Biomaterials 26 (2005) 2073–2080.
[7] H. Roussiere, F. Fayon, B. Alonso, T. Rouillon, V. Schnitzler, E. Verron, J. Guicheux, M. Petit, D. Massiot, P. Janvier, J.M. Bouler, B. Bujoli, Reaction of zoledronate with beta-tricalcium phosphate, for the design of potential drug device combined systems, Chem. Mater. 20 (2008) 182–191.
[8] E. Boanini, P. Torricelli, L. Forte, S. Pagani, N. Mihailescu, C. Ristoscu, I.N. Mihailescu, A. Bigi, Antiresorption implant coatings based on calcium alendronate and octacalcium phosphate deposited by matrix assisted pulsed laser evaporation, Colloid Surf. B-Biointerfaces 136 (2015) 449–456.
[9] E. Verron, I. Khairoun, J. Guicheux, J.M. Bouler, Calcium phosphate biomaterials as bone drug delivery systems: a review, Drug Discov. Today 15 (2010) 547–552.
[10] E. Verron, O. Gauthier, P. Janvier, P. Pilet, J. Lesoeur, B. Bujoli, J. Guicheux, J.M. Bouler, In vivo bone augmentation in an osteoporotic environment using bisphosphonate-loaded calcium deficient apatite, Biomaterials 31 (2010) 7776–7784.
[11] S. Panzavolta, P. Torricelli, B. Bracci, M. Fini, A. Bigi, Functionalization of biomimetic calcium phosphate bone cements with alendronate, J. Inorg. Biochem. 104 (2010) 1099–1106.
[12] E. Boanini, P. Torricelli, M. Gazzano, M. Fini, A. Bigi, The effect of zoledronate-hydroxyapatite nanocomposites on osteoclasts and osteoblast-like cells in vitro, Biomaterials 33 (2012) 722–730.
[13] F. Errassifi, S. Sarda, A. Barroug, A. Legrouri, H. Sfihi, C. Rey, Infrared, Raman and NMR investigations of risedronate adsorption on nanocrystalline apatites, J. Colloid Interface Sci. 420 (2014) 101–111.
[14] G.H. Nancollas, R. Tang, R.J. Phipps, Z. Henneman, S. Gulde, W. Wu, A. Mangood, R.G.G. Russell, F.H. Ebetino, Novel insights into actions of bisphosphonates on bone: differences in interactions with hydroxyapatite, Bone 38 (2006) 617–627.
[15] P. Pascaud, P. Gras, Y. Coppel, C. Rey, S. Sarda, Interaction between a bisphosphonate, tiludronate, and biomimetic nanocrystalline apatites, Langmuir 29 (2013) 2224–2232.
[16] P. Pascaud, F. Errassifi, F. Brouillet, S. Sarda, A. Barroug, A. Legrouri, C. Rey, Adsorption on apatitic calcium phosphates for drug delivery: interaction with bisphosphonate molecules, J. Mater. Sci. Mater. Med. 25 (2014) 2373–2381.
[17] Y. Murakami, K. Sugo, M. Hirano, T. Okuyama, Surface chemical analysis and chromatographic characterization of polyethylenimine-coated hydroxyapatite with various amount of polyethylenimine, Talanta 85 (2011) 1298–1303.
[18] A. Shkilnyy, A. Friedrich, B. Tiersch, S. Schöne, M. Fechner, J. Koetz, C.W. Släpfer, A. Taubert, Poly(ethylene imine)-controlled calcium phosphate mineralization, Langmuir 24 (2008) 2102–2109.
[19] V. Sokolova, S. Neumann, A. Kovtun, S. Chernousova, R. Heumann, M. Epple, An outer shell of positively charged poly(ethyleneimine) strongly increases the transfection efficiency of calcium phosphate/DNA nanoparticles, J. Mater. Sci. 45 (2010) 4952–4957.

[20] A. Bigi, E. Boanini, M. Gazzano, Ion substitution in biological and synthetic apatites, in: C. Aparicio, M.P. Ginebra (Eds.), Biomineralization and Biomaterials, Fundamentals and Applications, 1st ed., Woodhead Publishing (imprint Elsevier), 2015, pp. 235–266, ISBN: 9784233861782.

[21] D.V. Shepherd, K. Kauppinen, R.A. Brooks, S.M. Best, An in vitro study into the effect of zinc substituted hydroxyapatite on osteoclast number and activity, J. Biomed. Mater. Res. Part A 102 (2014) 4136–4141.

[22] A. Bigi, E. Boanini, M. Gazzano, M.A. Kojdecki, K. Rubini, Microstructural investigation of hydroxyapatite-polyelectrolyte composites, J. Mater. Chem. 14 (2004) 274–279.

[23] M. Ferrari, L. Lutterotti, Method for the simultaneous determination of anisotropic residual stresses and texture by X-ray diffraction, J. Appl. Phys. 76 (1994) 7246–7255.

[24] N.C. Popa, The (hkl) dependence of diffraction-line broadening caused by strain and size for all Laue groups in Rietveld refinement, J. Appl. Cryst. 31 (1998) 176–180.

[25] S. Lakard, G. Herlem, B. Lakard, B. Fahys, Theoretical study of the vibrational spectra of polyethylenimine and polypropylenimine, Theochem.-J. Mol. Struct. 685 (2004) 83–87.

[26] S. Gomes, J.M. Nedelec, G. Renaudin, On the effect of temperature on the insertion of zinc into hydroxyapatite, Acta Biomater. 8 (2012) 1180–1189.

[27] R.Q. Song, H. Cölfen, Mesocrystals—ordered nanoparticle superstructures, Adv. Mater. 22 (2010) 1301–1330.

[28] T.A. Fuierer, M. LoRe, S.A. Puckett, G.H. Nancollas, A mineralization adsorption and mobility study of hydroxyapatite surfaces in the presence of zinc and magnesium ions, Langmuir 10 (1994) 4721–4725.

[29] A. Bigi, E. Foresti, M. Gandolfi, M. Gazzano, N. Roveri, Inhibiting effect of zinc on hydroxylapatite crystallization, J. Inorg. Biochem. 58 (1995) 49–58.

[30] F. Ren, R. Xin, X. Ge, Y. Leng, Characterization and structural analysis of zinc-substituted hydroxyapatites, Acta Biomater. 5 (2009) 3141–3149.

[31] A. Al-Kattan, F. Errassifi, A.M. Sautereau, S. Sarda, P. Dufour, A. Barroug, I. Dos Santos, C. Combes, D. Grossin, C. Rey, C. Drouet, Medical potentialities of biomimetic apatites through adsorption, ionic substitution, and mineral/organic associations: three illustrative examples, Adv. Eng. Mater. 12 (2010) B224–B233.

[32] G. Penel, G. Leroy, C. Rey, E. Bres, MicroRaman spectral study of the PO_4 and CO_3 vibrational modes in synthetic and biological apatites, Calcif. Tissue Int. 63 (1998) 475–481.

[33] D. Eichert, C. Drouet, H. Sfihi, C. Rey, C. Combes, Nanocrystalline apatite-based biomaterials: synthesis processing and characterization, in: J.B. Kendall (Ed.), Biomaterials Research Advances, Nova Science Publishers, New York, 2008, pp. 93–143, ISBN: 9781600271892.

[34] P. Costa, J.M. Sousa Lobo, Modeling and comparison of dissolution profiles, Eur. J. Pharm. Sci. 13 (2001) 123–133.

[35] S. Hayakawa, In vitro degradation behavior of hydroxyapatite, in: M. Mucali (Ed.), Hydroxyapatite (Hap) for biomedical applications, Elsevier, 2015, pp. 85–105, ISBN: 9781782452041.

[36] R. Tang, W. Wu, M. Haas, G.H. Nancollas, Kinetics of dissolution of β-tricalcium phosphate, Langmuir 17 (2001) 3480–3485.

[37] M. Fatnassi, S. Jacquart, F. Brouillet, C. Rey, C. Combes, S. Girot Fullana, Optimization of spray-dried hyaluronic acid microspheres to formulate drug-loaded bone substitute materials, Powder Technol. 255 (2014) 44–51.

Supplementary Material

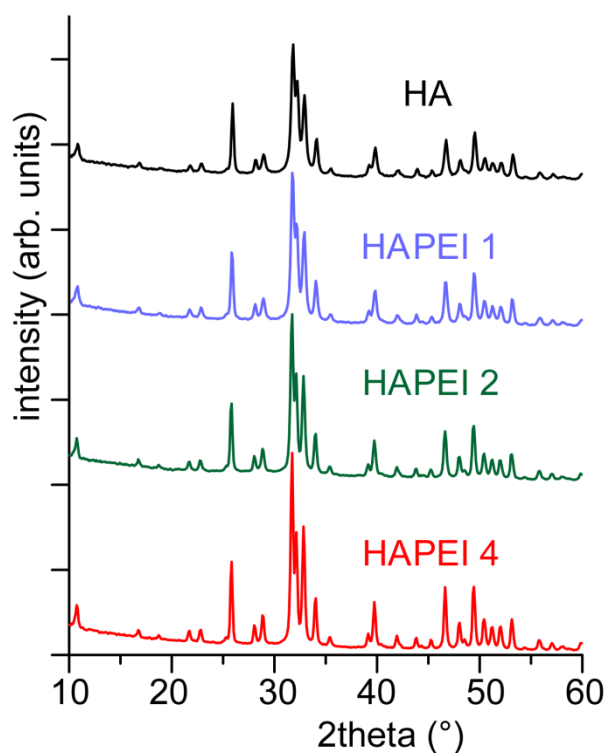# Hydroxyapatite functionalization to trigger adsorption and release of risedronate.

Lucia Forte, Stéphanie Sarda, Christèle Combes, Fabien Brouillet, Massimo Gazzano,

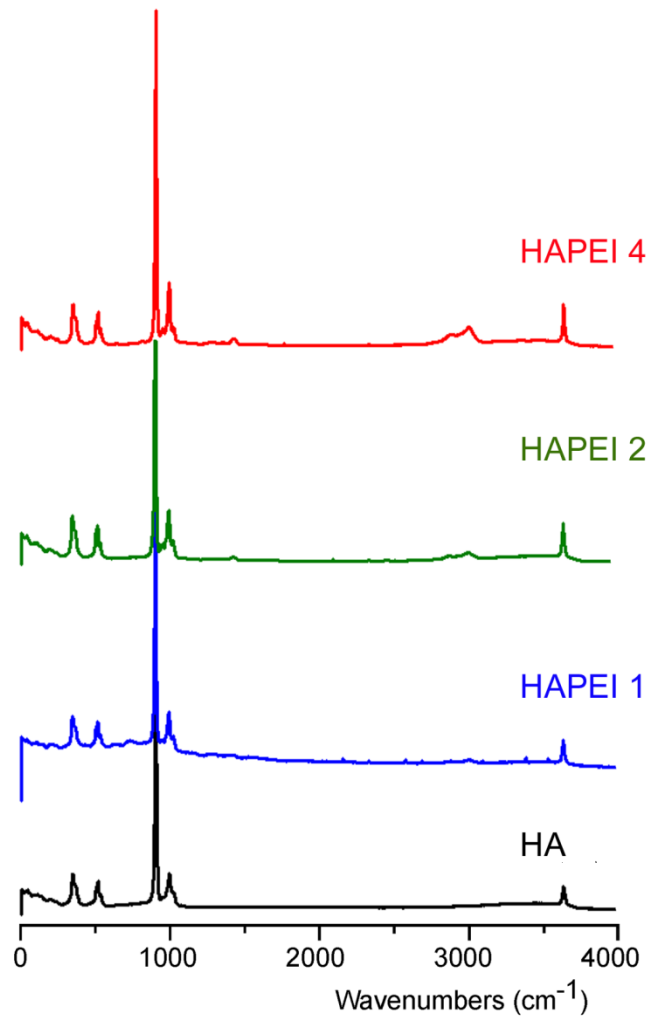Olivier Marsan, Elisa Boanini, Adriana Bigi
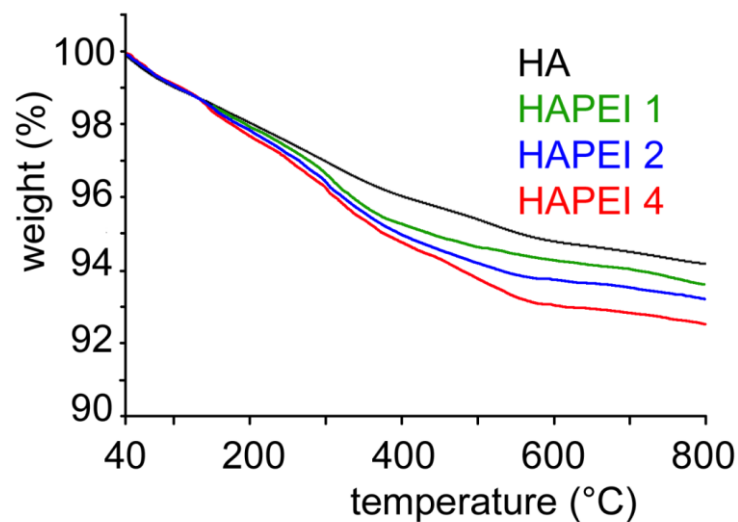
Content :

Figures S1 to S6

Table S1

Figure S1. Powder X-ray diffraction patterns of the apatitic samples synthesized in the presence of different PEI concentrations in solution (HAPEI 1, HAPEI 2 and HAPEI 4 for 1 M, 2 M and 4 M of PEI in solution, respectively), compared with HA (without PEI) XRD pattern.

Figure S2. Raman spectra of the apatitic samples synthesized with different PEI concentrations in solution (HAPEI 1, HAPEI 2 and HAPEI 4 for 1 M, 2 M and 4 M of PEI in solution, respectively), compared with HA spectrum.

Figure S3. Thermogravimetric plots of the apatitic samples synthesized in the presence of different PEI concentrations in solution (HAPEI 1, HAPEI 2 and HAPEI 4 for 1 M, 2 M and 4 M of PEI in solution, respectively), compared with HA sample (without PEI).
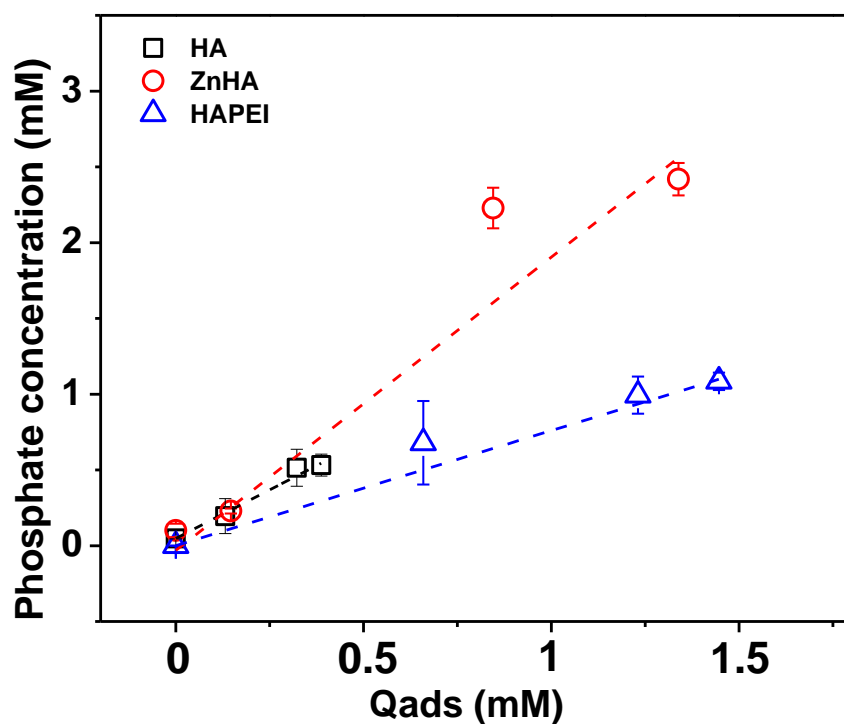

Figure S4. Concentration of phosphate ions in supernatants after adsorption of risedronate on HA, ZnHA and HAPEI.
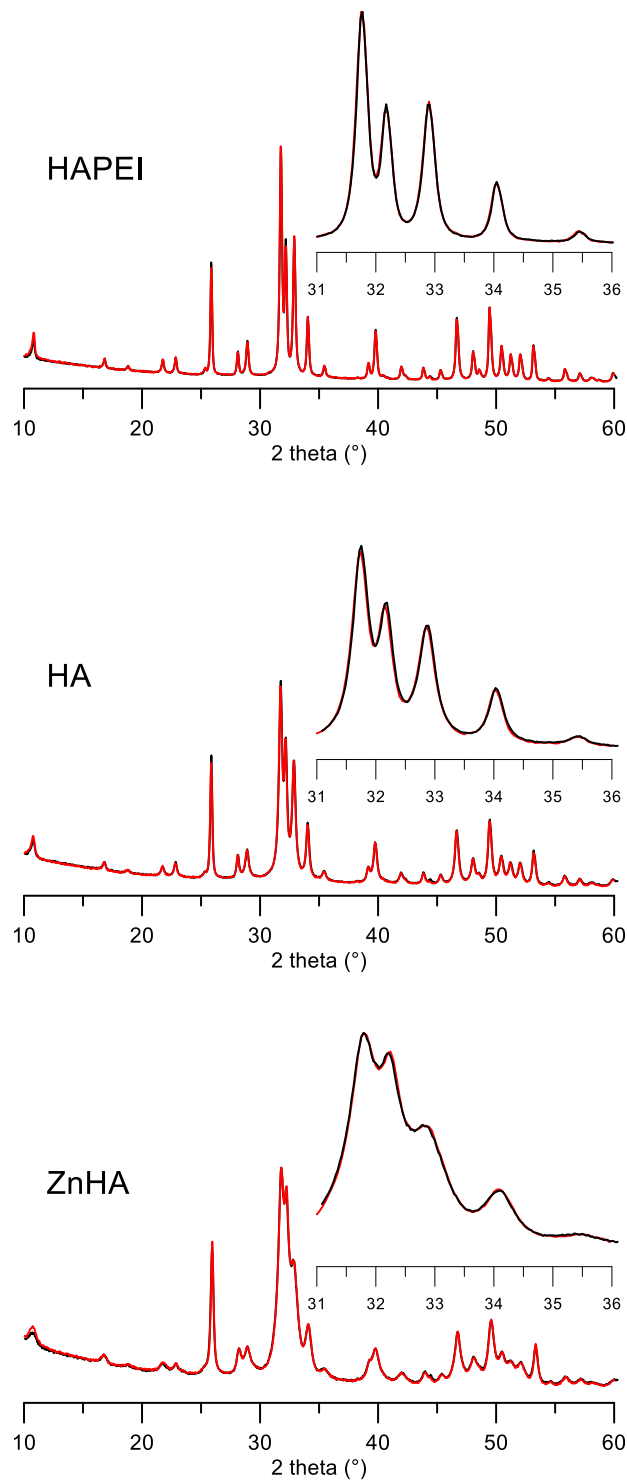
Figure S5. XRD patterns of apatitic samples before (black) and after (red) the adsorption process (in risedronate solution at 3 mM). No difference can be appreciated before and after the adsorption process, as it can be seen also in the insets, where the order of plotting has been reversed in order to highlight possible dissimilarity.
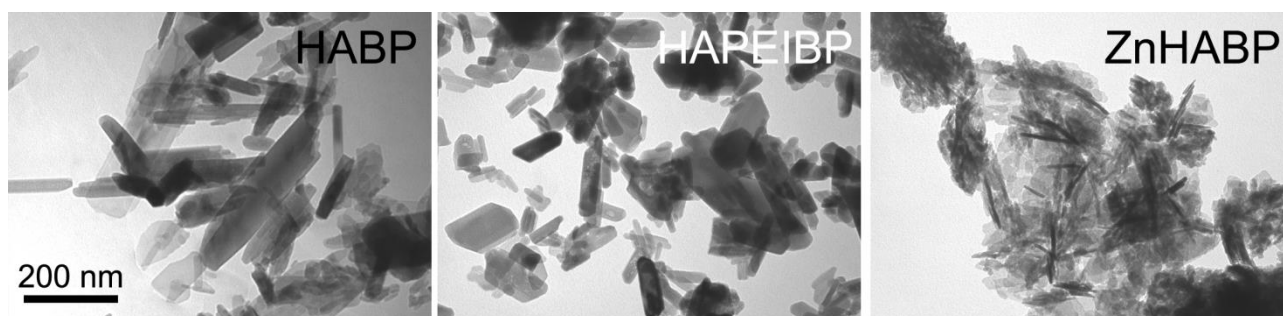
Figure S6. TEM images of the different apatite samples obtained after risedronate adsorption. Magnification is the same in all the images for direct comparison.

Table S1. Lattice parameters, coherent lengths (τL_{hkl}) of the perfect crystalline domains and microstrain (ε_{hkl}) in the direction normal to 002 and to 310 planes; PEI content, zeta potential and Ca/P molar ratio of the apatitic samples synthesized in the presence of different PEI concentrations in solution (HAPEI 1, HAPEI 2 and HAPEI 4 for 1 M, 2 M and 4 M of PEI in solution, respectively), compared with HA sample (without PEI).

	HA	HAPEI 1	HAPEI 2	HAPEI 4
a (Å)	9.4318(3)	9.4358(2)	9.4299(2)	9.4298(2)
c (Å)	6.8862(2)	6.8903(3)	6.8855(2)	6.8872(2)
L_{002} (Å)	657(4)	667(5)	749(6)	929(7)
L_{310} (Å)	311(3)	358(3)	405(4)	543(5)
ε_{002} (*10^{-4})	9.9(8.5)	6.9(5.1)	6.9(2.7)	5.9(7.0)
ε_{310} (*10^{-4})	6.0(1.2)	4.6(1.2)	6.2(2.3)	6.8(4.8)
PEI content (wt%)	---	0.9(0.5)	1.7(0.5)	2.4(0.5)
zeta potential (mV)	- 15.6	+ 19.5	+ 24.2	+ 26.2
Ca/P	1.67	1.67	1.67	1.73